

# Thermodynamic and Structural Analysis of Human NFU Conformational Chemistry

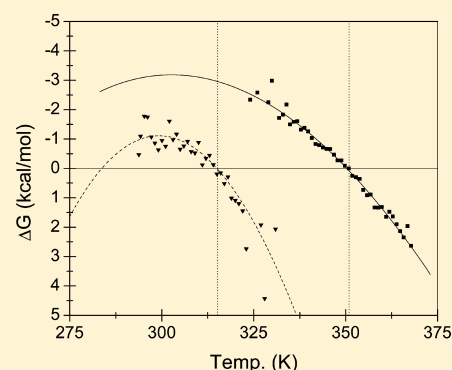
Jingwei Li,<sup>†</sup> Shu Ding,<sup>†</sup> and J. A. Cowan<sup>\*,†,‡</sup>

<sup>†</sup>Evans Laboratory of Chemistry, The Ohio State University, 100 West 18th Avenue, Columbus, Ohio 43210, United States

<sup>‡</sup>The Ohio State Biochemistry Program, The Ohio State University, 784 Biological Sciences, 484 West 12th Avenue, Columbus, Ohio 43210, United States

## S Supporting Information

**ABSTRACT:** Human NFU has been implicated in the formation of inorganic sulfide required for cellular iron–sulfur cluster biosynthesis. The protein contains a well-structured N-terminal domain and a C-terminal domain with molten globule characteristics that also contains a thioredoxin-like pair of redox active Cys residues that promote persulfide reductase activity. Recent reports have highlighted the existence of structural flexibility in the ISU/IscU-type scaffold proteins that mediate Fe–S cluster assembly, which is also likely to serve an important role in the pathway to Fe–S cluster maturation. We have previously reported similar structural mobility for the C-terminal domain of human NFU, a protein that has been implicated in the production of sulfide for cluster synthesis, while homologous proteins have also been suggested to serve as Fe–S cluster carriers. Herein we quantitatively characterize the structural stability of the two domains of human NFU and in particular the functional C-terminal domain. The results of differential scanning calorimetry and variable temperature circular dichroism (VTCD) studies have been used to analyze the temperature-dependent structural melting profiles of the N- and C-terminal domains, relative to both full-length NFU and an equimolar ratio of the N- and C-terminal domains, and correlated with structural information derived from NMR data. Calorimetry results indicate that the C-terminal NFU domain undergoes a significant structural stabilization following interaction with the N-terminal domain, which resulted in a novel and distinctive transition melting profile ( $T_m^{\text{sec}} = 58.1 \pm 0.4$  °C,  $\Delta H_v^{\text{sec}} = 60.4 \pm 5.3$  kcal/mol,  $T_m^{\text{ter}} = 49.3 \pm 0.3$  °C,  $\Delta H_v^{\text{ter}} = 71.8 \pm 5.8$  kcal/mol). VTCD experiments also revealed a secondary structure transition at 59.2 °C in agreement with calorimetry results. The degree of stabilization was found to be more significant in the full-length NFU, as the C-terminal domain transitions were recorded at higher temperatures ( $T_m^{\text{sec}} = 63.3 \pm 3.4$  °C,  $\Delta H_v^{\text{sec}} = 41.8 \pm 8.2$  kcal/mol). The interactions between the two domains demonstrated the hallmarks of a hydrophobic character, as increased ionic strength decreased the degree of stabilization of the C-terminal domain. An increase of 2% in  $\alpha$ -helix content further supports interaction between the two domains, leading to greater secondary structure stabilization. Heteronuclear single-quantum coherence experiments indicate that the C-terminal domain adopts an alternate tertiary conformation following binding to the N-terminal domain. The structural rigidity of the N-terminal domain leads to an alternative conformation of the C-terminal domain, suggesting that such an interaction, although weaker than that of the covalently attached native NFU, is important for the structural chemistry of the native full-length protein. The results also emphasize the likely general importance of such structural flexibility in select proteins mediating metal cofactor biosynthesis.



Human NFU is a multifunctional protein that has been demonstrated to interact with the histone cell cycle regulation homologue A (HIRA) as a transcriptional regulator because of its ability to influence chromatin structure.<sup>1,2</sup> Human NFU has also been linked to Lafora disease because of its interaction with laforin, a protein which is mutated in the disease state.<sup>3</sup> NFU family proteins have also been implicated in cellular iron–sulfur cluster biosynthesis, both in vivo and in vitro.<sup>4–11</sup> For example, the functional site<sup>11</sup> of human NFU is located in the C-terminal domain (C-NFU, 83 residues, Scheme 1) and shares significant sequence identity with Nfu in *Synechocystis* sp.,<sup>6</sup> Nfu1 in yeast,<sup>7,8</sup> and NfuA in *Azotobacter vinelandii*,<sup>10</sup> all of which have been reported to be involved in the iron–sulfur cluster assembly pathway within their

respective organisms. In some cases, Fe–S cluster binding has been noted and a possible role as an intermediate carrier of 2Fe or 4Fe Fe–S clusters has been proposed. For example, the Nfu-type protein from *Synechocystis* sp. has been reported in a 2Fe–2S form<sup>6</sup>, whereas *Escherichia coli* NfuA has also been demonstrated as an atypical carrier for 4Fe–4S clusters.<sup>9,10</sup> The conserved CXXC motif found in these proteins has also been identified in the C-terminal domain of NifU, the iron–sulfur cluster scaffold protein in the nitrogen fixation bacterial system.<sup>12</sup> Overall, the factors that promote cluster binding

Received: March 12, 2013

Revised: May 28, 2013

Published: June 24, 2013

**Scheme 1. NFU Sequence Showing the N-Terminal Domain in Bold and the C-Terminal Domain Underlined**

1	GSSHHHHHHS	<b>SGLVPRGSHM</b>	<b>FIQTQDTPNP</b>	<b>NSLKFIPGKP</b>	<b>VLETRTMDFP</b>	<b>TPAAAFRSPL</b>
61	<b>ARQLFRIEGV</b>	<b>KSVFFGPDFI</b>	<b>TVTKEEELD</b>	<b>WNLKPKDIYA</b>	<b>TIMDFFASGL</b>	<b>PLVTEETPSG</b>
121	<b>EAGSEEDDEV</b>	<b>VAMIKELLDI</b>	<b>RIRPTVQEDG</b>	<b>GDVIYKGFED</b>	<b>GIVQLKLQGS</b>	<b>CTSCPSSIIT</b>
181	<u>LKNGIQNMLQ</u>	<u>FYIPEVEGVE</u>	<u>QVMDESEDEK</u>	<u>EANSP</u>		

versus alternative functional roles remain unclear. The subject of this study, human NFU, possesses a C-terminal domain (C-NFU) that contains a pair of redox active cysteines that demonstrate thioredoxin-like activity.<sup>13,14</sup> This domain has been shown to bind and mediate persulfide bond cleavage of sulfur-loaded IscS, the sulfide donor protein in the final step of sulfide delivery for [2Fe-2S] cluster assembly on ISU-type scaffold proteins.<sup>15–17</sup> Alternative mechanisms of cysteinyl persulfide cleavage by NFU have also been proposed, including direct reduction via electrons derived from ferrous ions<sup>18</sup> and human ferredoxin (Fd),<sup>19</sup> as well as a possible role for oxidized Fd in removing electrons from the nascent reduced [2Fe-2S]<sup>+</sup> cluster.<sup>19</sup>

On the basis of an early report,<sup>20</sup> protein structural flexibility has emerged as an important theme in iron–sulfur cluster biosynthesis, particularly in the chemistry of the scaffold protein that promotes cluster assembly from iron and sulfide.<sup>20–25</sup> Previous studies have also revealed the C-terminal domain of human NFU to demonstrate molten globule-type structural behavior that may be of functional significance.<sup>13,26</sup> These studies included titration of full-length and truncated constructs of NFU with 1-anilino-8-naphthalenesulfonic acid (ANS), the kinetics of trypsin digestion, and heteronuclear single-quantum coherence (HSQC) NMR spectroscopy. By contrast, the N-terminal domain (N-NFU) retains a well-defined structure.

Herein, we describe a series of studies to further advance the understanding of the structural properties and thermal stabilities of N-NFU, C-NFU, full-length NFU (NFU), as well as a mixture of N-NFU and C-NFU (N-NFU/C-NFU). These studies provide additional support for an emerging theme in the biochemistry of iron–sulfur cluster biosynthesis,<sup>11,13,20–27</sup> namely, that key parts of the protein machinery underlying Fe–S cluster assembly must display structural flexibility in order to fully execute their functions in the context of a multistep process that could involve a variety of multiprotein complexes.<sup>21–25,28</sup> To advance this investigation, we have made use of differential scanning calorimetry (DSC), a thermal analytical technique that measures the heat capacity of a defined experimental sample, as well as variable temperature circular dichroism (VTCD) experiments in combination with high-field NMR spectroscopy. These bioanalytical methods provide not only information concerning the thermodynamic stability of proteins of interest but also more detailed information on the characteristics of intermediate states involved in melting and unfolding processes.<sup>29</sup>

## MATERIALS AND METHODS

**Expression and Purification of Human NFU.** Expression and purification of human NFU were performed from BL21 Lysozyme plus (DE3) competent cells as previously described.<sup>11,13,26</sup> In brief, 50 mL of LB culture (supplemented with 30 µg/mL kanamycin) was grown overnight followed by 1 L culture growth to an OD<sub>600</sub> of ~0.6 with subsequent addition of 1 mM IPTG for protein induction (3 h). The harvested cells were resuspended in Tris-buffer (50 mM Tris-HCl, pH 7.5) followed by sonication. The cell lysate was centrifuged by use of a Sorvall RC-5B Refrigerated Superspeed Centrifuge (Du Pont

Instruments) at 26890g and 4 °C for 30 min, and the resulting supernatant was loaded onto a TALON Metal Affinity Column (Clontech) equilibrated with Tris-buffer and eluted with 20 mM imidazole in Tris-buffer. The purity of the eluted protein was checked by sodium dodecyl sulfate–polyacrylamide gel electrophoresis, and the identity was confirmed by electrospray ionization mass spectrometry.

**Expression of <sup>15</sup>N-Labeled N-Terminal, C-Terminal, and Full-Length NFU.** For [<sup>15</sup>N–<sup>1</sup>H] HSQC analyses, <sup>15</sup>NH<sub>4</sub>Cl (99%, Cambridge Isotope Laboratory) supplemented M9 minimum medium (40 mM phosphate, 22 mM glucose, 20 mM <sup>14/15</sup>NH<sub>4</sub>Cl, 10 mM NaCl, 2 mM MgSO<sub>4</sub>, 0.1 mM CaCl<sub>2</sub>, 62 µM kanamycin) was used to express <sup>15</sup>N isotope-labeled proteins. In brief, newly transformed BL21 Lysozyme plus competent cells were grown in 20 mL of LB medium to an OD<sub>600</sub> of 1.0. After centrifugation, the cell pellet was resuspended in 0.5 L of unlabeled M9 medium and grown to an OD<sub>600</sub> of 0.8. The resulting cells were spun down and inoculated in 2 L of labeled M9 medium and grown to an OD<sub>600</sub> of 0.4, followed by IPTG induction (1 mM) for 3 h. Cell harvest and protein purification steps are described above.

**Differential Scanning Calorimetry.** All DSC samples (0.3 mM) were dialyzed against saline phosphate buffer (40 mM Na<sub>2</sub>HPO<sub>4</sub>, 100 mM NaCl, pH 7.4) or phosphate buffer (40 mM Na<sub>2</sub>HPO<sub>4</sub>, pH 7.4) with Spectra/Por dialysis membrane (MWCO 10 000; Spectrum Laboratories, Inc.). Resulting dialysis buffers were used as reference cell solvents for precision and repeatability. Prior to analyses, all sample and reference solutions were rigorously degassed with a Microcal Thermo-vac2 device (GE Healthcare). All DSC data were obtained on a MicroCal VP-DSC instrument (GE Healthcare) equipped with twin cells and operated on differential mode at a rate of 1.0 °C min<sup>−1</sup> from 15 to 90 or 110 °C. All data were processed with Origin 7 (Origin Laboratories) and fit according to a two-state model or non-two-state model with respect to individual data sets.<sup>30</sup>

**Nuclear Magnetic Resonance Spectroscopy.** [<sup>15</sup>N–<sup>1</sup>H] Heteronuclear single-quantum coherence (HSQC) spectra were recorded at The Ohio State University Campus Chemical Instrument Center. Samples (0.45 mM) were exchanged to phosphate buffer (40 mM Na<sub>2</sub>HPO<sub>4</sub>, 100 mM NaCl, pH 7.4) in 10% D<sub>2</sub>O by use of an Illustra MicroSpin G-25 column (GE Healthcare). A standard water suppression [<sup>15</sup>N–<sup>1</sup>H] HSQC pulse sequence was used for data collection,<sup>31</sup> followed by apodization, zero-filling, Fourier transformation, and phase correction. Detailed acquisition and processing parameters are listed in the Supporting Information, Table S1.

**Circular Dichroism Spectroscopy.** All circular dichroism (CD) samples (10 µM) were dialyzed to phosphate buffer (40 mM Na<sub>2</sub>HPO<sub>4</sub>, pH 7.4) with Spectra/Por dialysis membrane (MWCO 10 000; Spectrum Laboratories, Inc.). Resulting dialysis buffers were used as reference cell solvents for precision and repeatability. Prior to analyses, all sample and reference solutions were rigorously degassed with a Microcal Thermo-vac2 device (GE Healthcare). All CD data acquisitions were obtained on a JASCO J-815 CD spectrometer (JASCO) equipped with quartz cells with a 0.1 cm path length. Secondary

structure studies were conducted at eight averaging scans and 50 nm/min scan rate and monitored at 190–240 nm. The data were fit by K2D3 program (European Molecular Biology Laboratory).<sup>32</sup> Variable temperature studies were performed at a rate of 1.0 °C min<sup>-1</sup> from 20 to 95 °C. All data were processed with Origin 7 (Origin Laboratories). N-NFU and C-NFU VT data were fit to eq 1, while NC-NFU and full-length NFU VT data were fit to eq 2 for  $T_m$  and  $\Delta H_v$  determination.

$$\theta_{mr} = \left\{ \exp \left[ (1/-RT) \left( \Delta H_v \left( 1 - \frac{T}{T_m} \right) - C_p \left( (T_m - T) + T \ln \frac{T}{T_m} \right) \right) \right] / \left\{ 1 + \exp \left[ (1/-RT) \left( \Delta H_v \left( 1 - \frac{T}{T_m} \right) - C_p \left( (T_m - T) + T \ln \frac{T}{T_m} \right) \right) \right] \right\} \right\} (F - U) + U \quad (1)$$

where  $R$  is the ideal gas constant in calories per mole,  $T_m$  the melting temperature,  $\Delta H_v$  the van't Hoff enthalpy, and  $C_p$  the heat capacity, and  $F$  and  $U$  are the mean residue ellipticities ( $\theta_{mr}$ ) of the folded and unfolded protein, respectively.

$$\theta_{mr} = \left\{ \exp \left[ (1/-RT) \left( \Delta H_{v1} \left( 1 - \frac{T}{T_{m1}} \right) - C_{p1} \left( (T_{m1} - T) + T \ln \frac{T}{T_{m1}} \right) \right) \right] / \left\{ 1 + \exp \left[ (1/-RT) \left( \Delta H_{v1} \left( 1 - \frac{T}{T_{m1}} \right) - C_{p1} \left( (T_{m1} - T) + T \ln \frac{T}{T_{m1}} \right) \right) \right] \right\} \right\} (F - U_1) + \left\{ \exp \left[ (1/-RT) \left( \Delta H_{v2} \left( 1 - \frac{T}{T_{m2}} \right) - C_{p2} \left( (T_{m2} - T) + T \ln \frac{T}{T_{m2}} \right) \right) \right] / \left\{ 1 + \exp \left[ (1/-RT) \left( \Delta H_{v2} \left( 1 - \frac{T}{T_{m2}} \right) - C_{p2} \left( (T_{m2} - T) + T \ln \frac{T}{T_{m2}} \right) \right) \right] \right\} \right\} (U_1 - U_2) + U_2 \quad (2)$$

where the subscripts of  $T_m$ ,  $\Delta H_v$ , and  $C_p$  denote the transition parameters associated with the C- and N-terminal domains.

## RESULTS

**DSC Studies of N-Terminal Human NFU.** N-NFU DSC analyses were found to be in agreement with our previous NMR and CD studies<sup>26</sup> inasmuch as N-NFU displays a rigid,

well-behaved native structure at ambient temperature (Figure 1). The melting curve was analyzed and fit to a two-peak, non-

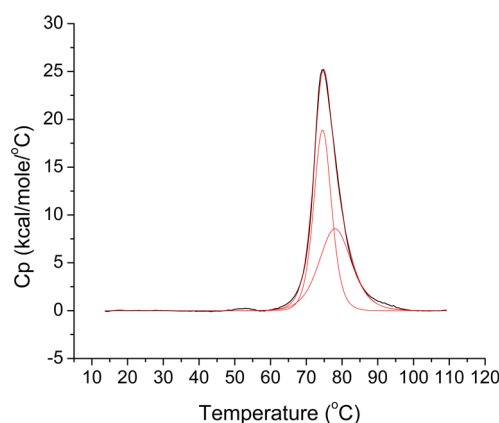


**Figure 1.** Differential scanning calorimetry profile for a 0.3 mM N-NFU solution in phosphate buffer. Origin was used to fit the data to a two-peak, non-two-state model (MN2State). Values for  $T_m$ ,  $\Delta H_{cal}$ , and  $\Delta H_v$  were obtained from the fit and are listed in Tables 1 and 2. The lower melting point was initialized at 79.4 °C, which was obtained from a VTCD analysis.

two-state model, yielding physical constants for melting temperatures ( $T_m$ ) of  $74.7 \pm 0.6$  and  $78.4 \pm 0.1$  °C (Table 1). The changes in molar enthalpy ( $\Delta H_{cal}$ ) and van't Hoff enthalpy ( $\Delta H_v$ ) from the fitting parameters were determined to be  $134.6 \pm 9.9$  and  $141.4 \pm 4.2$  kcal/mol for the lower transition and  $93.2 \pm 9.8$  and  $79.2 \pm 1.6$  kcal/mol for the higher transition, respectively (Table 2). The high  $T_m$  indicates the unfolding transitions for N-NFU stem from a well-folded state, while the reproducibility of melting for a sample following repetition of the heating cycle indicates that the melting process is reversible, but with partial protein degradation arising during each cycle (Supporting Information, Figure S1). This evidence suggests that at high temperature the N-NFU domain exists in a stable conformation and is able to fold back to the native state upon cooling.

**VTCD Studies of N-Terminal Human NFU.** The secondary structure of N-NFU was analyzed by CD spectroscopy, yielding a composition of 31%  $\alpha$ -helix, 21%  $\beta$ -sheet, and 48% random coil (Table 3). The K2D3 program<sup>32</sup> was used to obtain a prediction of secondary structure composition that was more accurate than previously possible.<sup>13</sup> Variable temperature studies yielded a structural transition at  $T_m = 79.5 \pm 0.4$  °C with  $\Delta H_v = 69.6 \pm 6.1$  kcal/mol (Figure 2, Tables 4 and 5), which is consistent with DSC results for secondary structure loss at 3.7 °C higher than the tertiary structure transition (Table 1).

**DSC Studies of C-Terminal Human NFU.** DSC analyses of the C-terminal domain of human NFU were consistent with a molten globule-like native structure<sup>26</sup> as the melting curve was observed to be broad and asymmetric over a span of 43 °C (Figure 3, top). Four transitions were calculated from the melting curve using the non-two-state model, with  $T_m$  values ranging from 55.0 to 72.9 °C. The first transition curve was observed to be broad, with  $\Delta H_{cal} > \Delta H_v$  in agreement with a molten globule-like native state structure. As the temperature increased, the calculated melting curves became sharper, resulting in  $\Delta H_{cal} < \Delta H_v$  for the transition at 72.9 °C. In conjunction with a negative peak observed at 74 °C, the

**Table 1. Melting Temperatures for N-Terminal NFU, C-Terminal NFU, a Mixture of N- and C-Terminal Domains, and Full-Length NFU Determined by DSC<sup>a</sup>**

	[NaCl] (mM)	$T_{m1}$ (°C)	$T_{m2}$ (°C)	$T_{m2} - T_{m1}$ (°C)	$T_{m3}$ (°C)	$T_{m4}$ (°C)	$T_{m4} - T_{m3}$ (°C)
N-NFU	100.0	74.7 ± 0.6	78.4 ± 0.1	3.7	—	—	—
	0.0	75.0 ± 0.6	80.0 ± 0.1	5.1	—	—	—
C-NFU	100.0	57–80	57–80	—	—	—	—
	0.0	49–81	49–81	—	—	—	—
N-NFU/C-NFU	100.0	49.3 ± 0.3	58.1 ± 0.4	8.8	78.0 ± 1.5	80.6 ± 0.2	2.6
	0.0	28.7 ± 0.7	41.4 ± 0.7	12.7	76.6 ± 0.5	80.9 ± 0.1	4.3
NFU	100.0	63.3 ± 3.4	67.0 ± 0.3	3.7	75.6 ± 7.9	77.1 ± 3.7	1.5
	0.0	51.3 ± 0.6	58.1 ± 2.6	6.7	69.4 ± 4.9	76.1 ± 1.2	6.7

<sup>a</sup>For a well-folded N-terminal domain, the change in melting temperatures for secondary and tertiary structures  $\Delta(T_{m}^{ter} - T_{m}^{sec})$  is inversely related to the ionic strength. The majority of this change is contributed by the decrease in  $T_{m}^{sec}$  at lower ionic strength.

**Table 2.  $\Delta H_{cal}$  and  $\Delta H_v$  for N-Terminal NFU, C-Terminal NFU, a Mixture of N- and C-Terminal Domains, and Full-Length NFU Determined by DSC<sup>a</sup>**

	[NaCl] (mM)	$\Delta H_{cal1}$ (kcal/mol)	$\Delta H_{v1}$ (kcal/mol)	$\Delta H_{cal2}$ (kcal/mol)	$\Delta H_{v2}$ (kcal/mol)	$\Delta H_{cal3}$ (kcal/mol)	$\Delta H_{v3}$ (kcal/mol)	$\Delta H_{cal4}$ (kcal/mol)	$\Delta H_{v4}$ (kcal/mol)
N-NFU	100	134.6 ± 9.9	141.4 ± 4.2	<b>93.2 ± 9.8</b>	<b>79.2 ± 1.6</b>	—	—	—	—
	0	<b>59.1 ± 3.6</b>	<b>52.8 ± 1.4</b>	66.2 ± 3.4	70.1 ± 4.1	—	—	—	—
C-NFU	100	—	—	—	—	—	—	—	—
	0	—	—	—	—	—	—	—	—
N-NFU/C-NFU	100	42.0 ± 0.4	71.8 ± 5.8	<b>40.9 ± 0.4</b>	<b>60.4 ± 5.3</b>	<b>68.2 ± 1.5</b>	<b>71.9 ± 4.9</b>	289.4 ± 1.5	128.4 ± 38.4
	0	28.3 ± 1.2	48.9 ± 2.9	<b>38.2 ± 1.2</b>	<b>42.9 ± 3.4</b>	<b>28.2 ± 0.5</b>	<b>28.3 ± 2.6</b>	194.4 ± 0.6	105.6 ± 2.5
NFU	100	94.0 ± 7.1	41.8 ± 8.2	<b>20.1 ± 7.6</b>	<b>36.9 ± 3.3</b>	125.7 ± 7.9	69.0 ± 45.1	37.9 ± 13.3	40.4 ± 2.7
	0	<b>29.6 ± 9.3</b>	<b>32.9 ± 11.6</b>	57.3 ± 8.9	49.1 ± 29.9	<b>28.3 ± 4.9</b>	<b>32.2 ± 15.4</b>	102.8 ± 4.4	67.9 ± 1.9

<sup>a</sup>Using the melting temperatures in Table 1 for comparison, the enthalpic contribution from the loss of secondary structure is listed in bold. In the cases of the N-NFU/C-NFU mixture and full-length NFU protein, two sets of enthalpies are observed because of the melting steps for the two independent domains.

**Table 3. Circular Dichroism Analyses of N-Terminal NFU, C-Terminal NFU, a Mixture of N- and C-Terminal Domains, and Full-Length NFU<sup>a</sup>**

	N-NFU	C-NFU	N-NFU/C-NFU		NFU
			experimental	theoretical	
$\alpha$ -helix	31%	30%	32%	30%	32%
$\beta$ -sheet	21%	16%	18%	18%	20%
random coil	48%	54%	50%	52%	48%

<sup>a</sup>Data were obtained at 25 °C with a path length of 0.1 cm and fit with the K2D3 program, which yields a  $\beta$ -strand prediction that is more accurate than that of its predecessor K2D. Theoretical values for the N-NFU/C-NFU mixture were calculated from the average values of the two isolated domains.

transitions at 70.0 and 72.9 °C suggest protein aggregation at elevated temperature. As expected, because of the structural instability of C-NFU, the melting and refolding cycle was irreversible as opposed to its N-NFU counterpart, and denatured precipitate was observed after a single heating ramp.

**VTCD Studies of C-Terminal Human NFU.** The thermal melting profile of the C-NFU secondary structure was monitored over the entire scanning range, from 20 to 95 °C (Figure 3, bottom, and Tables 4 and 5). The overall CD signal change was determined to be  $5.9 \pm 0.2$  mdeg. This is consistent with the DSC results that supported the low overall thermal stability of the C-NFU structure, which denatures over a broad range between 50 and 80 °C. Furthermore, the constant decrease of secondary structure (222 nm) over the entire heat ramp indicates multiple intermediates during melting, which is also consistent with DSC results using a four-state fitting model to define the structural loss. A single transition fit of the C-NFU

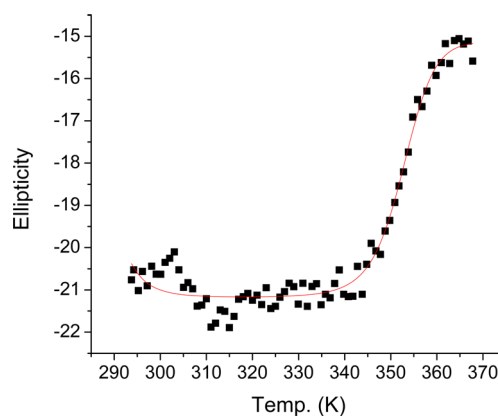


**Figure 2.** VTCD analysis of 10  $\mu$ M N-NFU in 40 mM phosphate, 100 mM NaCl buffer. Data were fit to eq 1 to yield values of  $\Delta H_v$ ,  $T_{m}^{sec}$ , and  $\Delta C_p$  of 69.56 kcal/mol, 79.44 °C, and 2.02 kcal mol<sup>-1</sup> K<sup>-1</sup>, respectively. Ellipticity data were directly used without converting to molar ellipticity units because the van't Hoff enthalpies are independent of such a factor.  $T_{m}^{sec}$  was used as an initial value for  $T_m$  in the DSC data-fitting routine.

melt resulted in a relatively low  $\Delta H_v$  ( $13.6 \pm 3.2$  kcal/mol), further indicating the absence of a distinct native state secondary structure.

**DSC and VTCD Studies of Full-Length Human NFU.** Two distinct secondary transitions were observed in VTCD profiles of NFU (Figure 4, bottom, and Tables 4 and 5). The transition at  $77.8 \pm 0.9$  °C is tentatively assigned to the N-terminal domain because of the similarity in  $T_m$  values in comparison to the N-NFU domain alone. The lower transition at  $67.8 \pm 0.8$  °C is likely due to the unfolding of the C-terminal



**Table 4. Melting Temperatures of N-Terminal NFU, C-Terminal NFU, a Mixture of N- and C-Terminal Domains, and Full-Length NFU Determined by VTCD<sup>a</sup>**

	[NaCl] (mM)	$T_{m1}$ (°C)	$T_{m2}$ (°C)
N-NFU	100.0	$79.5 \pm 0.4$	
	0.0	$75.7 \pm 0.1$	
C-NFU	100.0	$59.4 \pm 3.8$	
	0.0	$60.7 \pm 0.5$	
N-NFU/C-NFU	100.0	$59.2 \pm 0.5$	$78.6 \pm 0.2$
	0.0	$41.9 \pm 1.5$	$77.2 \pm 0.3$
NFU	100.0	$67.8 \pm 0.6$	$77.8 \pm 0.9$
	0.0	$50.2 \pm 1.2$	$71.0 \pm 0.4$

<sup>a</sup>The melting points were determined from molar ellipticity data fit with eq 1 or 2. As a result of the broad transitions observed for the C-NFU domain,  $T_m$  values were estimated according to a single transition. In rows containing data collected on a mixture of N-NFU/C-NFU and the full-length NFU, the  $T_{m1}$  and  $T_{m2}$  parameters refer to melting temperatures for the C-terminal and N-terminal domains, respectively.

**Table 5. Fitting Parameters for the Change in van't Hoff Enthalpy Determined by VTCD<sup>a</sup>**

	[NaCl] (mM)	$\Delta H_{v1}$ (kcal/mol)	$\Delta H_{v2}$ (kcal/mol)
N-NFU	100.0	$69.6 \pm 6.1$	
	0.0	$41.8 \pm 4.5$	
C-NFU	100.0	$13.6 \pm 3.2$	
	0.0	$17.7 \pm 0.9$	
N-NFU/C-NFU	100.0	$43.3 \pm 4.1$	$69.2 \pm 1.1$
	0.0	$44.1 \pm 4.5$	$45.8 \pm 0.7$
NFU	100.0	$23.9 \pm 1.7$	$41.0 \pm 2.7$
	0.0	$31.8 \pm 6.3$	$28.3 \pm 3.3$

<sup>a</sup>Values were obtained from fitting the molar ellipticity versus temperature by use of eq 1 or 2. Increasing ionic strength resulted in an increase in the van't Hoff enthalpy, indicating a relatively more stable secondary structure for well-folded domains, such as N-NFU, and consistent with the trends observed in the melting temperatures defined in Table 4.

domain because it corresponds to the lowest thermally stable domain for NFU. The van't Hoff enthalpies associated with the N-terminal and C-terminal domains were determined to be  $41.0 \pm 2.7$  and  $23.9 \pm 1.7$  kcal/mol, respectively. The distinct transition observed for the C-terminal domain at its  $T_m$ , together with the increased melting  $\Delta H_v$  relative to C-NFU alone, suggests that the secondary structure of this domain is stabilized in NFU.

The thermal melting curve of NFU (Figure 4, top) indicates a convoluted transition with  $T_m$  near 72 °C. Using the secondary structure unfolding  $\Delta H_v$  value determined by the VTCD, the DSC plot was fit to four peaks that correspond to the loss of secondary and tertiary structure of the N- and C-terminal domains of the NFU. In comparison with the DSC melting curves from the N-terminal domain (Figure 1) and the C-terminal domain (Figure 3, top), two of the four peaks of the NFU melting curve correspond to the individual domains of the full-length protein; the higher  $T_m$  value of  $77.1 \pm 3.7$  °C corresponds to melting of the N-NFU domain, whereas the lower  $T_m$  value of  $67.0 \pm 0.3$  °C corresponds to unfolding of the C-NFU domain. The relatively modest difference between  $\Delta H_{cal}$  and  $\Delta H_v$  for both transitions is characteristic of two-state unfolding processes, suggesting the absence of melting intermediates or protein aggregation of the individual domains

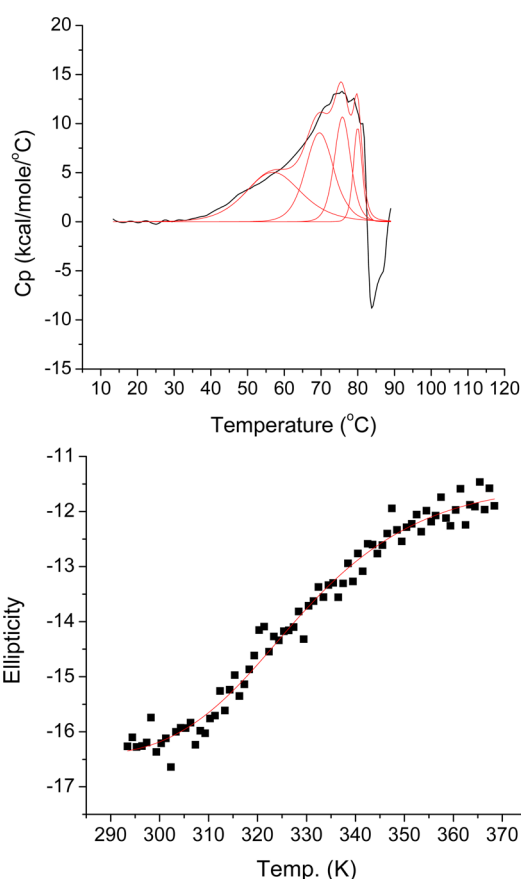


**Figure 3.** DSC and VTCD analysis of C-NFU in 40 mM phosphate, 100 mM NaCl buffer. (Top) Upscan of 0.3 mM C-NFU from 10 to 90 °C with a rate of 1 K min<sup>-1</sup> recorded by DSC. (Bottom) Upscan of 10 μM C-NFU with the same conditions monitored at 222 nm by CD. VTCD data were fit to eq 1, and results are listed in Tables 4 and 5. Fitting results from DSC experiments are listed in Tables 1 and 2.

in the full-length protein. Furthermore, the similarity of the two enthalpies in NFU compared with those of the individual domains, along with the reversibility of melting (Supporting Information, Figure S1), suggests that in forming the full-length protein, both domains have been structurally stabilized. These changes in thermodynamic and structural properties are more significant for the C-NFU domain, as forming the complete protein apparently alters its native state and results in a relatively more structurally ordered macromolecule. The C-NFU domain in NFU is thermally well-behaved as the fitting yielded an overall melting  $\Delta H_{cal}$  of  $114.1 \pm 10.8$  kcal/mol (Table 2). We speculate that in the full-length protein, the C-terminal domain is stabilized by the N-terminal domain and therefore exhibits significant tertiary structure in comparison to the isolated domain.

**DSC Studies of a Mixture of N- and C-Terminal Domains of NFU.** The DSC results described thus far demonstrate unusual but interesting interactions between the N- and C-terminal domains of NFU. To further elucidate the chemistry between the two segments, we carried out DSC studies on solution mixtures of equimolar N-NFU and C-NFU (Figure 5, top), which yielded three noteworthy observations. First, the transitions at  $T_m$  values of  $49.3 \pm 0.3$  and  $58.1 \pm 0.4$  °C correspond to unfolding of C-NFU in the solution mixture. The overall structural behavior of C-NFU in the presence of N-NFU was observed to be more stable, with a symmetric melting

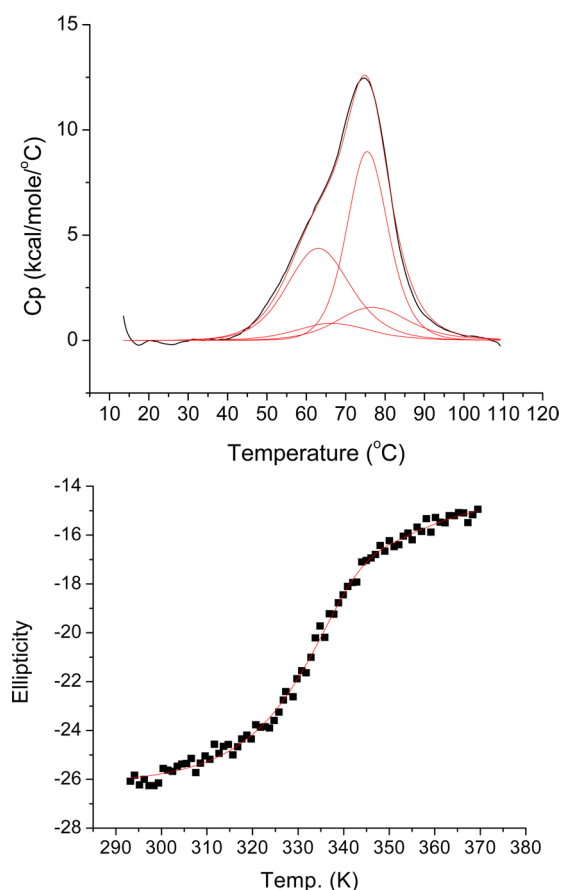


**Figure 4.** DSC and VTCD analysis of NFU in 40 mM phosphate and 100 mM NaCl buffer. (Top) Upscan of 0.3 mM NFU from 10 to 110 °C at a rate of 1 K min<sup>-1</sup> recorded by DSC. (Bottom) Upscan of 10 μM NFU under the same conditions, but monitored at 222 nm by CD. VTCD data were fit to eq 2, and results are listed in Tables 4 and 5. Fitting results from DSC experiments are listed in Tables 1 and 2.

profile and  $\Delta H_{\text{cal}} \approx \Delta H_v$ . Furthermore, the secondary and tertiary structural  $T_m$  values observed for C-NFU in solution with N-NFU are  $8.93 \pm 0.5$  and  $14.04 \pm 3.4$  °C lower than that of the C-NFU domain of the full-length NFU protein, respectively, indicating that the degree of structural stabilization by N-NFU is stronger when the two domains are covalently attached. The interaction surface between the two domains is likely to be dominated by hydrophobic interactions, because decreasing buffer ionic strength was observed to weaken the degree of thermal stabilization of C-NFU. This is consistent with the results of isothermal titration calorimetry studies in which no significant enthalpic response was observed by titrating the two domains.<sup>13</sup> Rather, any binding would have to be promoted by entropy-driven interactions. Lastly, interaction between the two domains increases the overall structural stability of the N-terminal domain, which can be observed from the increased  $T_m$  and an overall increase of  $129.7 \pm 14.1$  kcal/mol in molar enthalpy.

**VTCD Studies of a Mixture of N- and C-Terminal Domains of NFU.** Similar to that of NFU, the VTCD melting curve of a mixture of N-NFU and C-NFU showed two distinct transitions (Figure 5, bottom, and Table 4). The lower transition was observed at  $59.2 \pm 0.5$  °C and corresponds to the C-NFU secondary structure melt. In comparison to the VTCD profile for C-NFU alone, the thermal transition was observed to be well-behaved with  $\Delta H_v = 43.3 \pm 4.1$  kcal/mol in

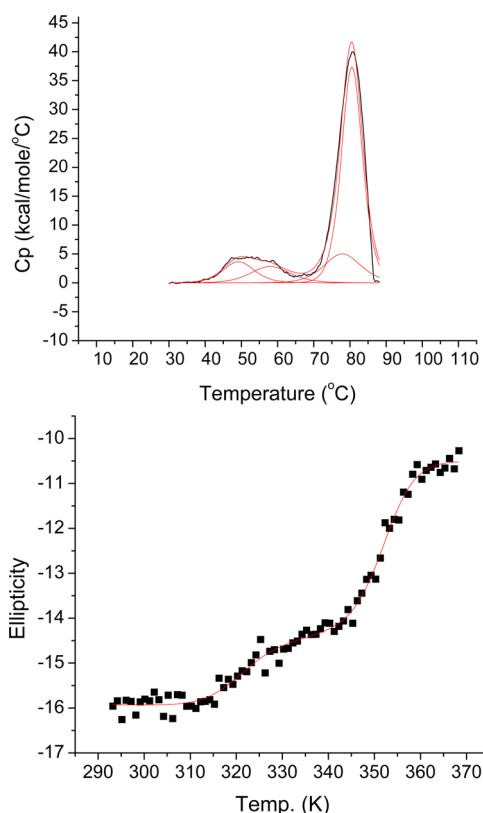


**Figure 5.** DSC and VTCD analysis of a N-NFU/C-NFU mixture in 40 mM phosphate and 100 mM NaCl buffer. (Top) Upscan of a mixture of 0.3 mM N-NFU and C-NFU from 10 to 90 °C at a rate of 1 K min<sup>-1</sup> recorded by DSC. (Bottom) Upscan of a 10 μM mixture of 0.3 mM N-NFU and C-NFU under the same conditions, but monitored at 222 nm by CD.

the presence of N-NFU (Table 5), which is more than 3-fold greater than that of the C-NFU-only VTCD melting curve. The thermodynamic parameters evaluated for C-NFU are in agreement with its DSC profile and estimated melting enthalpies and support the conformational change and structural stabilization of C-NFU following binding to N-NFU.

**[<sup>15</sup>N–<sup>1</sup>H] HSQC Studies of a Mixture of N- and C-Terminal Domains of NFU.** To further study the interaction between N-NFU and C-NFU, each of the two domains was prepared in a <sup>15</sup>N-isotopically enriched form. First, comparing the spectra from the isolated <sup>15</sup>N-N-NFU domain and either an equimolar mixture of <sup>15</sup>N-N-NFU and <sup>14</sup>N-C-NFU or the <sup>15</sup>N-labeled full-length protein (Supporting Information, Figure S8) revealed no shifted cross-peaks and no significant change in the conformation of the N-terminal domain. That is, the structure appears conserved both as the isolated N-NFU in complex with C-NFU and as a separate domain in the full-length NFU protein. By contrast, experiments conducted with the C-terminal C-NFU domain under the same solution conditions as the DSC analyses demonstrated very distinct behavior. When equimolar mixtures of <sup>14</sup>N-N-NFU and <sup>15</sup>N-C-NFU were mixed and studied by [<sup>15</sup>N–<sup>1</sup>H] HSQC NMR experiments, a comparison of the spectrum relative to that obtained for the isolated <sup>15</sup>N-labeled C-NFU domain revealed 21 new <sup>15</sup>N–<sup>1</sup>H cross-peaks (Figure 6A,B and Supporting Information, Table S2). These peaks suggest an alternative tertiary conformation for C-NFU following interaction with the N-NFU domain. Furthermore, the observed new peaks exhibit distinct chemical

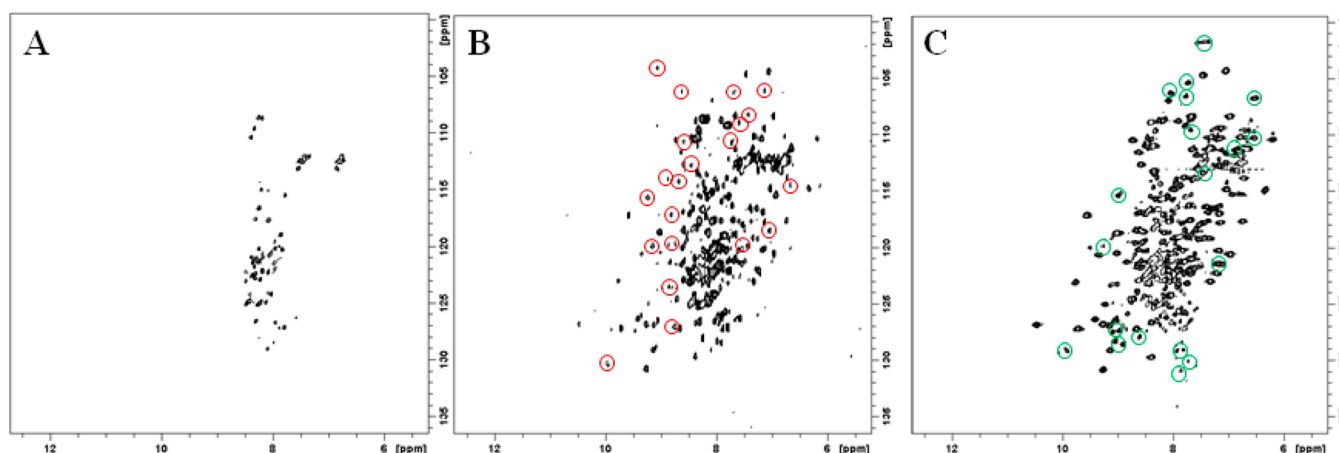


**Figure 6.**  $^1\text{H}$ – $^{15}\text{N}$  HSQC spectra of (A)  $^{15}\text{N}$ -C-NFU, (B)  $^{14}\text{N}$ -N-NFU +  $^{15}\text{N}$ -C-NFU, and (C)  $^{15}\text{N}$ -NFU. The C-terminal domain undergoes structural change in the presence of the N-terminal domain, as reflected by the peaks circled in red in (B). Cross-peaks are also observed in spectrum (B) from the non-enriched N-NFU domain as a result of the natural abundance of  $^{15}\text{N}$ , providing an effective comparison of spectra for full-length NFU (C) relative to the sum of the individual domains (B). The cross-peaks circled in green in spectrum (C) highlight the chemical shifts of the full-length protein that are unique from the individual domains and in some cases overlap with the peaks from the structure-stabilized C-terminal domain. Chemical shifts for new cross-peaks identified in (B) and (C) are listed in Supporting Information, Tables S2 and S3, respectively.

shifts that span the chemical shift range from 6.67 to 9.96 ppm in the  $^1\text{H}$  domain, and from 103.98 to 130.27 ppm in the  $^{15}\text{N}$  domain, supporting a conformational change in C-NFU with a greater level of tertiary structure and corresponding diversity in the chemical environment of its residues. When the spectrum for the  $^{15}\text{N}$ -labeled C-NFU domain was compared to that for the  $^{15}\text{N}$ -labeled full-length NFU (Figure 6A,C), 23 new cross-peaks were observed (Supporting Information, Table S3). Significantly, only four of those new cross peaks found for C-NFU in the full-length NFU protein were co-localized with cross-peaks observed in the spectrum for the mixture of the  $^{14}\text{N}$ -N-NFU and  $^{15}\text{N}$ -C-NFU domains (Supporting Information, Table S3, bold). Apparently the structural transition induced by complex formation between the isolated N-NFU and C-NFU domains is incomplete, relative to the two domains in the full-length NFU protein.

## DISCUSSION

Comparison of the two isolated domains of the full-length NFU protein has shown the N-terminal fragment to display higher thermal stability relative to its C-NFU counterpart (Figure 1 and Figure 3, top, respectively). This is consistent with our previous studies demonstrating the N-terminus of NFU to possess a more rigid conformation than the C-terminal NFU.<sup>26</sup> The C-terminal domain exhibits molten globule characteristics with lower thermostability (Figure 3, bottom) and does not display a well-folded tertiary structure according to both CD and NMR criteria.<sup>11,13,26</sup> DSC studies of C-NFU reported herein revealed structural heterogeneity during the unfolding process (Figure 3, top), while the VTCD melt showed a consistent decrease in secondary structure throughout the temperature domain (Figure 3, bottom). The ability of N-NFU to promote conformational change and stabilize the structure of C-NFU was confirmed by both DSC and CD melting experiments (Figure 5) and 2D-NMR experiments (Figure 6). The degree of stabilization was observed to be greater for full-length NFU, relative to a mixture of the two domains (Figure 6B vs 6C). The secondary structures of the N-NFU/C-NFU mixture contain 2% less random coil than the expected composition, which is consistent with the sharp CD melting

curve due to the new C-NFU conformation (Figure 5, bottom). Although N-NFU somewhat stabilizes the secondary and tertiary structure of C-NFU, there remains a significant amount of molten globular C-NFU within the mixture of the two proteins, with 50% random coil present in the secondary structure (Table 3). Increasing ionic strength is known to stabilize the thermostability of molten globules.<sup>33</sup> Accordingly, the difference in the degree of structural stabilization between these two cases is also reflected in the results of DSC studies using a lower ionic strength buffer (0 mM NaCl), where a decrease of 18.6 °C was observed in the  $T_m$  value for C-NFU in the mixture of proteins, but only 10.5 °C in NFU (Table 1). Furthermore, by comparing the  $^{15}\text{N}$ – $^1\text{H}$  HSQC NMR spectrum of full-length NFU to that from a mixture of the N-NFU and C-NFU domains, we observed 23 new cross-peaks (Figure 6C and Supporting Information, Figure S7), relative to the 21 new peaks observed for C-NFU following N-NFU binding in the co-complex of the two domains (Figure 6B and Supporting Information, Figure S6), although only 4 of these new cross-peaks from each spectrum are found to co-localize (Supporting Information, Tables S2 and S3). These residues underline the difference between the N/C-domain protein–protein interaction and covalently attached NFU. Nevertheless, the ability of N-NFU to structurally stabilize C-NFU was demonstrated in both cases through the appearance of new cross-peaks in the NMR experiments (Figure 6) and is consistent with the progressive changes observed in the DSC plots for each isolated domain, relative to the mixture of domains and full-length protein (Figures 1–5).

The Gibbs free energy for the secondary structural transition was converted from CD melt data using eq 3 and drawn to illustrate the unfolding profile for N-NFU (Figure 7).

$$\Delta G = -RT \ln \frac{\theta_{\text{mr}} - U}{F - \theta_{\text{mr}}} \quad (3)$$

According to the plot, as temperature increases, the  $\Delta G$  response is first observed to increase as the melting process is enthalpy driven. The free energy  $\Delta G$  reaches the highest value at ~37 °C because N-NFU is most likely thermostable at physiological temperatures. The unfolding free energy

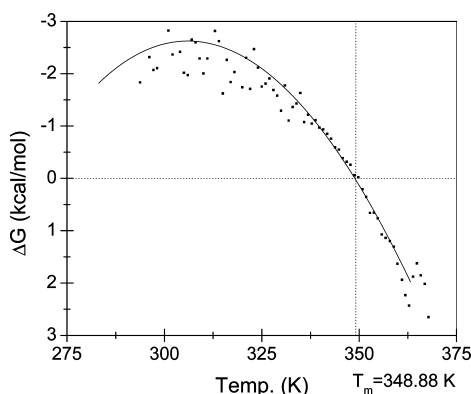


**Figure 7.** Thermal profile for N-NFU. Data (dots) were converted to  $\Delta G$  values by use of eq 3, and the Gibbs–Helmholtz equation along with  $\Delta H_v$ ,  $T_m^{\text{sec}}$ , and  $\Delta C_p$  was used to form a plot of  $\Delta G$  versus temperature (line). As expected, N-NFU is most thermally stable near human body temperature, while melting of the protein is a favorable process at temperatures exceeding 79.4 °C.

decreases as the temperature increases from 37 to 78 °C because the unfolding process is entropy driven. Figure 8 shows the thermal profile of a mixture of N- and C-NFU, and NFU, to be similar to the N-NFU thermal profile, where all thermal transitions were fit to yield a  $\Delta G_{\text{max}}$  near 37 °C.

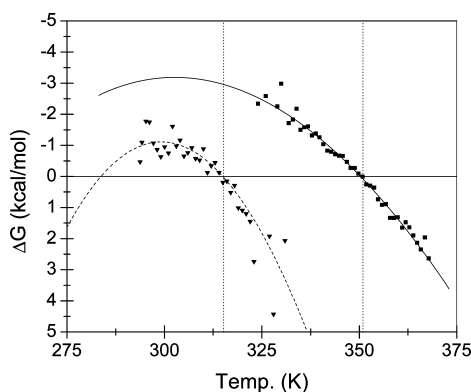


**Figure 8.** Gibbs free energy plot illustrates a mixture of N-NFU and C-NFU domains to be most thermally stable near physiological temperature. The solid line represents the calculated data for N-NFU, and the dashed line the calculated data for C-NFU. Squares (■) show the experimental data for N-NFU, and triangles (▼) show the experimental data for C-NFU. The vertical dashed lines indicate the fitted  $T_m$  values of C-NFU (315.0 K) and N-NFU (350.3 K).

The influence of N-NFU on C-NFU underlines the importance of the structural role of the N-terminal domain in the native structure of NFU. In agreement with our previous studies, the N-terminal domain appears to maintain the overall structure of the full-length protein.<sup>11,13,26</sup> We conclude that hydrophobic interactions between the N- and C-terminal domains facilitate the folding of each, illustrated by the observation that the unfolding of C-NFU changes from a molten globule state to a relatively more thermally stable conformation. However, the C-terminal domain in the full-length protein is not fully structured as observed by NMR experiments.<sup>26</sup> This is also supported by the increased thermostability of the C-terminal domain under high-salt conditions. Structural disorder is generally considered to be a factor that decreases enzyme catalytic efficiency. However,

recent reports have shown molten globular enzymes adopting functional conformations upon binding to relevant binding partners or ligands, such as the case of chorismate mutase.<sup>34</sup> Similarly, the molten globular C-terminal domain of NFU may adopt its functional conformation upon binding to sulfur donors and subsequently aid in the 2Fe–2S cluster assembly with scaffolding proteins. As demonstrated by both ITC and kinetic studies, human NFU is known to bind to IscS in the process of reconstitution of human ISU scaffold protein.<sup>13</sup> In order for the conserved CXXC thiolate groups to reduce the persulfide bond on IscS and subsequently relocate sulfide ions into the ISU active site, it is likely that the C-NFU adopts a distinct and more structured conformation. The absence of a thermally stable tertiary conformation for the C-terminal CXXC domain may provide the required structural flexibility to allow such a reaction. The decrease in flexibility of C-NFU in the presence of N-NFU was also observed in the secondary structure predictions, with an increase in ~2%  $\alpha$ -helix content (5 residues) upon binding. A recent bioinformatic study reported that a majority of protein–protein interactions are due to helix interactions (62%) with involvement commonly between 4 and 14 residues,<sup>35</sup> such as the bacterial Barnase–Barstar system.<sup>36</sup> The Zimm–Bragg theory describes that the rate-determining step in formation of  $\alpha$ -helix is the formation of the first loop, which requires ~20 kcal. However, the subsequent helix growth is exothermic and a thermodynamically favored process. Therefore, the formation of additional  $\alpha$ -helix content between the two termini of NFU is likely to be entropy driven and forms spontaneously, leading to alternative secondary and tertiary conformations for the C-terminal domain.

## CONCLUSION

The term molten globule is ascribed to a diverse category of protein structural conformations that are broadly defined by a high degree of secondary structure, but lacking a rigid tertiary structure.<sup>37,38</sup> There are many examples for alternative conformers with distinct recognition or functional roles within a given protein molecule.<sup>39–41</sup> Calorimetry results and our previous investigations<sup>13,26</sup> suggest that the C-terminal domain of human NFU exists in a molten globule state both in the truncated form and within the full-length protein, but with different conformations and physical properties. The C-terminal domain appears to adopt an alternative conformation following interaction with the N-terminal domain. This change in conformation is accompanied by an increase in the tertiary structure as well as an increase in thermostability. This property of structural flexibility most likely underlies the required properties and functions of the protein, as also observed in the cases of molten globular clusterin and nucleosomes.<sup>42</sup> Interestingly, the iron–sulfur scaffold protein *Thermotoga maritima* IscU appears to equilibrate between structural conformers and may be essential for its interactions with various protein partners.<sup>20</sup> Structural isomerism within this family of scaffold proteins has also been emphasized by recent work from the Markley group.<sup>21–25</sup> Because of the complexity of iron–sulfur cluster assembly systems and numerous contributions from scaffold, partner, and chaperone proteins, we propose that a dynamic tertiary structure is an important factor for the proper functioning of several key proteins involved in Fe–S cluster formation.



## ■ ASSOCIATED CONTENT

### ■ Supporting Information

Details of protein expression and purification and CD, DSC, and NMR experiments. This material is available free of charge via the Internet at <http://pubs.acs.org>.

## ■ AUTHOR INFORMATION

### Corresponding Author

\*Evans Laboratory of Chemistry, The Ohio State University, 100 W. 18th Ave., Columbus, OH 43210. Tel: 614-292-2703. E-mail: [cowan@chemistry.ohio-state.edu](mailto:cowan@chemistry.ohio-state.edu).

### Funding

This work was supported by a grant from the National Institutes of Health (AI072443).

### Notes

The authors declare no competing financial interest.

## ■ ABBREVIATIONS

ANS, 1-anilino-8-naphthalenesulfonic acid; CD, circular dichroism; DSC, differential scanning calorimetry; HIRA, histone cell cycle regulation homologue A; IPTG, isopropyl- $\beta$ -D-thiogalactopyranoside; HSQC, heteronuclear single-quantum coherence; Isc, iron-sulfur cluster; ITC, isothermal titration calorimetry; LB, Luria-Bertani; MWCO, molecular weight cutoff; PAGE, polyacrylamide gel electrophoresis; Tris, tris-(hydroxymethyl)aminomethane; VTCD, variable temperature circular dichroism

## ■ REFERENCES

- (1) Lorain, S.; Lecluse, Y.; Scamps, C.; Mattei, M. G., and Lipinski, M. (2001) Identification of human and mouse HIRA-interacting protein-5 (HIRIP5), two mammalian representatives in a family of phylogenetically conserved proteins with a role in the biogenesis of Fe/S proteins. *Biochim. Biophys. Acta* 1517, 376–383.
- (2) Magnaghi, P.; Roberts, C.; Lorain, S.; Lipinski, M., and Scambler, P. J. (1998) HIRA, a mammalian homologue of *Saccharomyces cerevisiae* transcriptional co-repressors, interacts with Pax3. *Nat. Genet.* 20, 74–77.
- (3) Ganesh, S.; Tsurutani, N.; Suzuki, T.; Ueda, K.; Agarwala, K. L.; Osada, H.; Delgado-Escueta, A. V., and Yamakawa, K. (2003) The Lafora disease gene product laforin interacts with HIRIP5, a phylogenetically conserved protein containing a NifU-like domain. *Hum. Mol. Genet.* 12, 2359–2368.
- (4) Tong, W. H.; Jameson, G. N.; Huynh, B. H., and Rouault, T. A. (2003) Subcellular compartmentalization of human Nfu, an iron-sulfur cluster scaffold protein, and its ability to assemble a [4Fe–4S] cluster. *Proc. Natl. Acad. Sci. U.S.A.* 100, 9762–9767.
- (5) Nishio, K., and Nakai, M. (2000) Transfer of Iron-Sulfur Cluster from NifU to Apoferritin. *J. Biol. Chem.* 275, 22615–22618.
- (6) Nakamura, Y.; Kaneko, T.; Hirose, M.; Miyajima, N., and Tabata, S. (1998) CyanoBase, a www database containing the complete nucleotide sequence of the genome of *Synechocystis* sp. strain PCC6803. *Nucleic Acids Res.* 26, 63–67.
- (7) Schilke, B.; Voisine, C.; Beinert, H., and Craig, E. (1999) Evidence for a conserved system for iron metabolism in the mitochondria of *Saccharomyces cerevisiae*. *Proc. Natl. Acad. Sci. U.S.A.* 10206.
- (8) Garland, S. A.; Hoff, K.; Vickery, L. E., and Culotta, V. C. (1999) *Saccharomyces cerevisiae* ISU1 and ISU2: Members of a well-conserved gene family for iron-sulfur cluster assembly. *J. Mol. Biol.* 294, 897–907.
- (9) Py, B.; Gerez, C.; Angelini, S.; Planel, R.; Vinella, D.; Brochier-Amanet, C.; Serres, R. G.; Latour, J.-M.; Choudens, S. O.; Fontecave, M., and Barras, F. (2012) Molecular organization, biochemical function, cellular role and evolution of NfuA, an atypical Fe-S carrier. *Mol. Microbiol.* 86, 155–171.

- (10) Bandyopadhyay, S.; Naik, S. G.; O'Carroll, I. P.; Huynh, B. H.; Dean, D. R.; Johnson, M. K., and Dos Santos, P. C. (2008) A proposed role for the *Azotobacter vinelandii* NfuA protein as an intermediate iron-sulfur cluster carrier. *J. Biol. Chem.* 283, 14092–14099.
- (11) Liu, Y., and Cowan, J. A. (2007) Iron sulfur cluster biosynthesis. Human NFU mediates sulfide delivery to ISU in the final step of [2Fe–2S] cluster assembly. *Chem. Commun.*, 3192–3194.
- (12) Yuvaniyama, P.; Agar, J. N.; Cash, V. L.; Johnson, M. K., and Dean, D. R. (2000) NifS-directed assembly of a transient [2Fe–2S] cluster within the NifU protein. *Proc. Natl. Acad. Sci. U.S.A.* 97, 599–604.
- (13) Liu, Y.; Qi, W., and Cowan, J. A. (2009) Iron-sulfur Cluster Biosynthesis: Functional Characterization of the N- and C-Terminal Domains of Human NFU. *Biochemistry* 48, 973–980.
- (14) Frazzon, J.; Fick, J. R., and Dean, D. R. (2002) Biosynthesis of iron-sulfur clusters is a complex and highly conserved process. *Biochem. Soc. Trans.* 30, 680–685.
- (15) Dean, D. R.; Bolin, J. T., and Zheng, L. M. (1993) Nitrogenase Metalloclusters—Structures, Organization, and Synthesis. *J. Bacteriol.* 175, 6737–6744.
- (16) Gerber, J.; Muhlenhoff, U., and Lill, R. (2003) An interaction between frataxin and Isu1/Nfs1 that is crucial for Fe/S cluster synthesis on Isu1. *EMBO Rep.* 4, 906–911.
- (17) Mansy, S. S., and Cowan, J. A. (2004) Iron-Sulfur Cluster Biosynthesis: Toward an Understanding of Cellular Machinery and Molecular Mechanism. *Acc. Chem. Res.* 37, 719–725.
- (18) Muhlenhoff, U.; Richhardt, N.; Gerber, J., and Lill, R. (2002) Characterization of iron-sulfur protein assembly in isolated mitochondria. A requirement for ATP, NADH, and reduced iron. *J. Biol. Chem.* 277, 29810–29816.
- (19) Li, J.; Saxena, S.; Pain, D., and Dancis, A. (2001) Adrenodoxin Reductase Homolog (Arh1p) of Yeast Mitochondria Required for Iron Homeostasis. *J. Biol. Chem.* 276, 1503.
- (20) Mansy, S. S.; Wu, S. P., and Cowan, J. A. (2004) Iron-Sulfur Cluster Biosynthesis: Biochemical characterization of the conformational dynamics of *Thermotoga maritima* IscU and the relevance for cellular cluster assembly. *J. Biol. Chem.* 279, 10469–10475.
- (21) Dai, Z.; Tonelli, M., and Markley, J. L. (2012) Metamorphic Protein IscU Changes Conformation by *cis-trans* Isomerizations of Two Peptidyl-Prolyl Peptide Bonds. *Biochemistry* 51, 9595–9602.
- (22) Fuzery, A. K.; Oh, J. J.; Ta, D. T.; Vickery, L. E., and Markley, J. L. (2011) Three hydrophobic amino acids in *Escherichia coli* HscB make the greatest contribution to the stability of the HscB-IscU complex. *BMC Biochem.* 12, 1–9.
- (23) Kim, J. H.; Tonelli, M.; Frederick, R. O.; Chow, D. C. F., and Markley, J. L. (2012) Specialized Hsp70 Chaperone (HscA) Binds Preferentially to the Disordered Form, whereas J-protein (HscB) Binds Preferentially to the Structured Form of the Iron-Sulfur Cluster Scaffold Protein (IscU). *J. Biol. Chem.* 287, 31406–31413.
- (24) Kim, J. H.; Tonelli, M., and Markley, J. L. (2012) Disordered form of the scaffold protein IscU is the substrate for iron-sulfur cluster assembly on cysteine desulfurase. *Proc. Natl. Acad. Sci. U.S.A.* 109, 454–459.
- (25) Markley, J. L.; Kim, J. H.; Dai, Z.; Bothe, J. R.; Cai, K.; Frederick, R. O., and Tonelli, M. (2013) Metamorphic protein IscU alternates conformations in the course of its role as the scaffold protein for iron-sulfur cluster biosynthesis and delivery. *FEBS Lett.* 587, 1172–1179.
- (26) Liu, Y., and Cowan, J. A. (2009) Iron-Sulfur Cluster Biosynthesis: Characterization of a Molten Globule Domain in Human NFU. *Biochemistry* 48, 7512–7518.
- (27) Ramelot, T. A.; Cort, J. R.; Goldsmith-Fischman, S.; Kornhaber, G. J.; Xiao, R.; Shastry, R.; Acton, T. B.; Honig, B.; Montelione, G. T., and Kennedy, M. A. (2004) Solution NMR structure of the iron-sulfur cluster assembly protein U (IscU) with zinc bound at the active site. *J. Mol. Biol.* 344, 567–583.
- (28) Cowan, J. A. (2009) Iron Sulfur Cluster Biosynthesis: Scaffold and Donor Proteins, and Mechanistic Insights. *ACS Symp. Ser.* 1012, 3–16.

- (29) Spink, C. H. (2008) Differential Scanning Calorimetry. In *Biophysical Tools for Biologists, Vol 1: in Vitro Techniques* (Correia, J. J., and Detrich, H. W., III, Eds.) pp 115–141, Academic Press, Amsterdam.
- (30) Sturtevant, J. M. (1987) Biochemical Applications of Differential Scanning Calorimetry. *Annu. Rev. Phys. Chem.* 38, 463–488.
- (31) Mori, S., Abeygunawardana, C., O’Neil-Johnson, M., and van Zijl, P. C. M. (1995) Improved sensitivity of HSQC spectra of exchanging protons at short interscan delays using a new fast HSQC (FHSQC) detection scheme that avoids water saturation. *J. Magn. Reson.* 108, 94–98.
- (32) Louis-Jeune, C., Andrade-Navarro, M. A., and Perez-Iratxeta, C. (2011) Prediction of protein secondary structure from circular dichroism using theoretically derived spectra. *Proteins* 80, 374–381.
- (33) Nishii, I., Kataoka, M., and Goto, Y. (1995) Thermodynamic stability of the molten globule states of apomyoglobin. *J. Mol. Biol.* 250, 223–238.
- (34) Pervushin, K., Vamvaca, K., Vogeli, B., and Hilvert, D. (2007) Structure and dynamics of a molten globular enzyme. *Nat. Struct. Mol. Biol.* 14, 1202–1206.
- (35) Jochim, A. L., and Paramjit, S. A. (2009) Assessment of helical interfaces in protein-protein interactions. *Mol. Biosyst.* 5, 924–926.
- (36) Buckle, A. M., Schreiber, G., and Fersht, A. R. (1994) Protein–Protein Recognition: Crystal Structural Analysis of a Barnase–Barstar Complex at 2.0-Å Resolution. *Biochemistry* 33, 8878–8889.
- (37) Ohgushi, M., and Wada, A. (1983) ‘Molten-globule state’: A compact form of globular proteins with mobile side-chains. *FEBS Lett.* 164, 21–24.
- (38) Kuwajima, K. (1977) A folding model of  $\alpha$ -lactalbumin deduced from the three-state denaturation mechanism. *J. Mol. Biol.* 114, 241–258.
- (39) Wilson, G., Ford, S. J., Cooper, A., Hecht, L., Wen, Z. Q., and Barron, L. D. (1995) Vibrational Raman optical activity of  $\alpha$ -lactalbumin: Comparison with lysozyme, and evidence for native tertiary folds in molten globule states. *J. Mol. Biol.* 254, 747–760.
- (40) Fink, A. L. (1995) Compact intermediate states in protein folding. *Annu. Rev. Biophys. Biomol. Struct.* 24, 495–522.
- (41) Creighton, T. E. (1990) Protein folding. *Biochem. J.* 270, 1–16.
- (42) Dunker, A. K., Lawson, J. D., Brown, C. J., Williams, R. M., Romero, P., Oh, J. S., Oldfield, C. J., Campen, A. M., Ratliff, C. M., Hipps, K. W., Ausio, J., Nissen, M. S., Reeves, R., Kang, C., Kissinger, C. R., Bailey, R. W., Griswold, M. D., Chiu, W., Garner, E. C., and Obradovic, Z. (2001) Intrinsically disordered protein. *J. Mol. Graphics Modell.* 19, 26–59.